Biomaterials 69 (2015) 1–11

Contents lists available at ScienceDirect

Biomaterials

journal homepage: www.elsevier.com/locate/biomaterials

Regulating the surface poly(ethylene glycol) density of polymeric nanoparticles and evaluating its role in drug delivery in vivo

Xiao-Jiao Du [a, 1], Ji-Long Wang [a, 1], Wei-Wei Liu [a, 1], Jin-Xian Yang [b], Chun-Yang Sun [a], Rong Sun [b], Hong-Jun Li [a], Song Shen [a], Ying-Li Luo [a], Xiao-Dong Ye [b, **], Yan-Hua Zhu [a], Xian-Zhu Yang [a], Jun Wang [a, b, *]

[a] The CAS Key Laboratory of Innate Immunity and Chronic Disease, School of Life Sciences and Medical Center, University of Science and Technology of China, Hefei, Anhui 230027, China
[b] Hefei National Laboratory for Physical Sciences at the Microscale, University of Science and Technology of China, Hefei, Anhui 230027, China

ARTICLE INFO

Article history:
Received 14 April 2015
Received in revised form
24 July 2015
Accepted 31 July 2015
Available online 1 August 2015

Keywords:
Polymeric nanoparticles
Self-assembly
PEGylation
Biological behaviors
Drug delivery
Cancer therapy

ABSTRACT

Poly(ethylene glycol) (PEG) is usually used to protect nanoparticles from rapid clearance in blood. The effects are highly dependent on the surface PEG density of nanoparticles. However, there lacks a detailed and informative study in PEG density and in vivo drug delivery due to the critical techniques to precisely control the surface PEG density when maintaining other nano-properties. Here, we regulated the polymeric nanoparticles' size and surface PEG density by incorporating poly(ε-caprolactone) (PCL) homopolymer into poly(ethylene glycol)-block-poly(ε-caprolactone) (PEG–PCL) and adjusting the mass ratio of PCL to PEG–PCL during the nanoparticles preparation. We further developed a library of polymeric nanoparticles with different but controllable sizes and surface PEG densities by changing the molecular weight of the PCL block in PEG–PCL and tuning the molar ratio of repeating units of PCL (CL) to that of PEG (EG). We thus obtained a group of nanoparticles with variable surface PEG densities but with other nano-properties identical, and investigated the effects of surface PEG densities on the biological behaviors of nanoparticles in mice. We found that, high surface PEG density made the nanoparticles resistant to absorption of serum protein and uptake by macrophages, leading to a greater accumulation of nanoparticles in tumor tissue, which recuperated the defects of decreased internalization by tumor cells, resulting in superior antitumor efficacy when carrying docetaxel.

© 2015 Elsevier Ltd. All rights reserved.

1. Introduction

Successful application of nanoparticles in intravenous administration usually requires a hydrophilic surface coating, and PEGylation is generally regarded as the superior approach used to create "stealth" nanoparticles, which reduces nonspecific cellular uptake by the mononuclear phagocyte system (MPS) and modulates the circulation half-life of nanoparticles [1–4]. Several examples, including Doxil and Genexol-PM as used in clinical practice, are PEGylated nanoparticles [5–7].

The effectiveness of "stealth" behavior of PEG-modified nanoparticles is often critically dependent on the density and conformation of surface PEG chains [8–11]. Some previous research explored the relationship of surface PEG densities with their in vivo biological behaviors, using PEGylated inorganic nanoparticles (like gold [12,13], silica [14], carbon [15], iron oxide [16] etc.) or polymeric nanoparticles prepared by a template method [17]. For example, Chan et al. obtained nanoparticles with different surface PEG densities by mixing different contents of PEG–SH with gold nanoparticles, and confirmed that increasing surface PEG density could significantly reduce the total amount of serum protein adsorption, which resulted in weak uptake by macrophages [18]. DeSimone et al. prepared polymeric nanoparticles using the PRINT method, and then modified the surface of these nanoparticles with PEG by means of chemical reaction [17]. They defined the morphology of PEG molecules in low surface density as a "mushroom" conformation, and PEG in high surface density as a "brush"

* Corresponding author. The CAS Key Laboratory of Innate Immunity and Chronic Disease, School of Life Sciences and Medical Center, University of Science and Technology of China, Hefei, Anhui 230027, China.
** Corresponding author.
E-mail addresses: xdye@ustc.edu.cn (X.-D. Ye), jwang699@ustc.edu.cn (J. Wang).
[1] These authors contributed equally to this work.

http://dx.doi.org/10.1016/j.biomaterials.2015.07.048
0142-9612/© 2015 Elsevier Ltd. All rights reserved.

conformation, and pointed out that nanoparticles with a "brush" PEG conformation could significantly prolong the blood circulation time as compared to a "mushroom" PEG conformation. Although the studies using inorganic materials and cross-linked polymeric nanoparticles show guidance on the design of nanoparticles, the information is still limited with regard to the PEGylation of self-assembled nanoparticles in drug delivery.

Due to the technical hurdles in quantifying the extent of PEG densities, as well as in regulating the surface PEG density while maintaining other nano-properties unchanged, for polymeric self-assembled nanoparticles, there is only a small amount of research on the relationship of surface PEG densities with their in vivo drug delivery properties [19–21]. In order to achieve the aim of changing the surface PEG densities of polymeric nanoparticles, researchers have usually incorporated hydrophobic homopolymer into the relative block copolymer. For example, Gref et al. adjusted surface PEG densities by adding different masses of polylactide (PLA) into poly(ethylene glycol)-block-polylactide (PEG–PLA) during nanoparticle preparations, but this also caused significant particle size change [19]. However, it should be pointed out that the in vivo fate of drug delivery systems are greatly associated with multiple physical and chemical properties of nanoparticles, including size, surface chemistry, surface charge, shape and so on [22–26]. It is generally considered that nanoparticles with small size (<10 nm) are rapidly cleared in blood circulation by filtration through the kidneys, while particles larger than 300 nm are more likely to be taken up by Kupffer cells in the liver [27–29]. In addition, Fang et al. have reported that the blood clearance of nanoparticles with a diameter of 80 nm was twice as slow as that of larger nanoparticles with a diameter of 171 or 243 nm [30]. Perrault et al. demonstrated that nanoparticles with an approximate 100 nm diameter deliver more cargoes to the tumor compared to those with 20, 40, 60 and 80 nm diameters [31]. Cabral et al. found that smaller nanoparticles showed better penetration in poorly permeable tumors and achieved better antitumor efficiency [32]. Therefore, in the study of surface PEG density of nanoparticles and its role in their in vivo behaviors, other nano-properties should be kept identical to avoid unreliable conclusions.

To circumvent these challenges and gain improved systemic insight into the relationship between surface PEG densities and their behaviors in biological environments as well as their antitumor efficacy, in this study we developed a library of polymeric nanoparticles with controllable surface PEG densities and sizes, by combining PEG–PCL copolymer and PCL homopolymer in the preparations, from which we selected a group of nanoparticles with varying surface PEG densities but similar sizes in order to study the effect of surface PEG density on the in vivo fate of nanoparticles in mice. The size of nanoparticles was controlled by regulating the mass ratio of PCL homopolymer incorporated into PEG–PCL, and PEG density was also judiciously modulated by changing the molecular weight of PEG–PCL and the molar ratio of repeating units of PCL (CL) to that of PEG (EG). This approach enabled PEG chains on nanoparticles at sufficient densities to achieve not only "brush" but even "dense brush" conformations. Using these well-characterized nanoparticles, we systematically explored the effect of surface PEG density on nanoparticles' in vivo fate and antitumor efficacy.

2. Materials and methods

2.1. Materials

Methoxy poly(ethylene glycol) (MW = 3400 Da) was purchased from Shanghai Jingyu Biotechnology Co., Ltd (China). ε-Caprolactone (ε-CL, Daicel Corporation, Japan) was dried over calcium hydride for 48 h at room temperature, followed by distillation under reduced pressure just before use. The diblock copolymer of monomethoxy poly(ethylene glycol) and poly(ε-caprolactone) (PEG–PCL) was synthesized and characterized as previously reported [33]. $PCL_{3.5k}$ homopolymer was synthesized by ring-opening polymerization of ε-caprolactone with aluminum isopropoxide as the initiator according to a previously reported method [34]. N,N′-Diisopropylcarbodiimide (DIC), 4-dimethylaminopyridine (DMAP) and Rhodamine B (RhoB) were purchased from Aladdin Industrial Inc. (China). PCL-RhoB was synthesized by a condensation reaction. $PCL_{3.5K}$ (500 mg, 1.0 eqv), Rhodamine B (211 mg, 3.0 eqv), DIC (55 mg, 5.0 eqv) and DMAP (55 mg, 5.0 eqv) were dissolved in 10 mL DMF and stirred at room temperature in the dark. After 2 d, the mixture was submitted to dialysis in DMF with dialysis bag (MWCO = 1000). The solution was collected until the colorless perinephric fluid appeared. The product was concentrated under reduced pressure and obtained as a deep pink solid (yield: 70%). Docetaxel (DTXL) was purchased from Knowshine (Shanghai) Pharmachemicals Inc. (China). All other reagents and solvents without statement were of analytical grade and used as received.

2.2. Preparation of polymeric nanoparticles

Polymeric nanoparticles were prepared by a dialysis method as follows: PEG–PCL copolymer was dissolved in acetonitrile (20 mg/mL) in a round-bottomed flask, except for $PEG_{3.4k}$–PCL_{12k}, which was dissolved in tetrahydrofuran (THF). After stirring for 10 min at room temperature, three volumes of Milli-Q ultrapure water (Millipore, 18.2 MΩ, Bedford, MA) were added under vigorous stirring. The mixture was stirred for another 20 min at room temperature. Afterwards, the solution was dialyzed against ultrapure water overnight with a dialysis bag (Spectra/Por®, Float-A-Lyzer, molecular cutoff (MWCO) = 14,000 Da) to remove acetonitrile, then the nanoparticles were stored at 4 °C for further use. Particle size and zeta-potential were measured using a Malvern Zetasizer Nano ZS90 dynamic light scattering system (DLS), with a He–Ne (633 nm) and 90° collecting optics. The data were analyzed by Malvern Dispersion Technology Software 7.0.2. The surface morphology of micelles was detected by transmission electron microscopy (TEM), on a JEOL 2010 high-resolution transmission electron microscopy with an accelerating voltage of 200 kV.

For the purpose of regulating the size of polymeric nanoparticles, $PCL_{3.5k}$ homopolymer was incorporated into PEG–PCL copolymer when preparing the nanoparticles. The sum of the weights of PEG–PCL and $PCL_{3.5K}$ was kept constant (12 mg), while the molar ratio of PCL homopolymer to PEG–PCL was changed.

In order to obtain nanoparticles with same size and different surface PEG density, we synthesized a series of PEG–PCL copolymers of $PEG_{3.4k}$ and PCL block with different molecular weights, and then prepared nanoparticles using these PEG–PCL copolymers and $PCL_{3.5K}$ homopolymer under different ratios.

Fluorescent-labeled nanoparticles were obtained by replacing part of $PCL_{3.5k}$ homopolymer with $PCL_{3.5k}$-RhoB when preparing the nanoparticles.

2.3. Static light scattering measurements

A commercial LLS spectrometer (ALV/DLS/SLS-5022F) equipped with a multi-τ digital time correlation (ALV5000) and a cylindrical 22-mW He–Ne laser (λ_0 = 632 nm, UNIPHASE) as the light source was used. Polymeric nanoparticles with a concentration of 0.3–0.9 mg/mL in Milli-Q ultrapurified water were clarified by a 0.45 μm hydrophilic PTFE filter (Millipore, Bedford, MA) into a dust-free vial and carried out at 20.0 °C. The average molecular weight of an individual micelle (Mw) was determined by measurements of SLS.

2.4. Cell lines and animals

The human breast cancer cell line MDA-MB-231, human melanoma cell line B16 and murine macrophage cell line RAW264.7 were obtained from the American Type Culture Collection. The MDA-MB-231 cell line with stably expressing green fluorescent protein (MDA-MB-231-GFP) was obtained by transfection with a retrovirus according to a standard protocol, and clones derived from discrete colonies were isolated and amplified in the medium. Both of these cells were cultured in a DMEM medium (Gibco, Grand Island, USA) supplemented with 10% fetal bovine serum (FBS, ExCell Bio, Shanghai, China) and 1% penicillin/streptomycin (Sigma–Aldrich, St. Louis, USA).

Female BALB/c nude mice, ICR mice and C57BL/6J mice (6–8 weeks) were purchased from the Beijing HFK Bioscience Co., Ltd. (Beijing, China). All animals received care in compliance with the guidelines outlined in the Guide for the Care and Use of Laboratory Animals, and all procedures were approved by the University of Science and Technology of China Animal Care and Use Committee.

To establish the xenograft breast tumor model, 100 μL of MDA-MB-231 or MDA-MB-231-GFP cells (2×10^6) diluted in 20% matrigel (BD Bioscience, Franklin Lakes, NJ) were injected into the mammary fat pad of the BALB/c nude mice. The subcutaneous melanoma tumor model was generated by injection of B16 (2×10^5 cells/100 μL) into the right flank of C57BL/6J mice.

2.5. Pharmacokinetic studies

The pharmacokinetics was measured using six to eight week-old female ICR mice. Rhodamine B-labeled nanoparticles were dissolved in phosphate buffered saline (PBS, 0.01 M, pH 7.4) and administrated intravenously into the tail vein at an equivalent dose of 360 μg $PCL_{3.5k}$-RhoB per kg of mouse body weight ($n = 4$ for each group). After a predetermined time (0.083, 0.5, 1, 2, 4, 6, 12, 24 and 48 h), blood samples were collected from the retro-orbital plexus of mouse eyes and were added into a heparin anticoagulant tube before coagulation. Then the blood was centrifuged at 3000 g for 10 min to obtain the plasma. For analysis, the plasma (100 μL) was exposed to 200 μL of acetonitrile. After vortexing for 10 s, 800 μL of chloroform was added on another vortex-mixer for 10 s. Upon centrifugation at 10,000 g for 5 min, the organic layer was carefully collected into 1.5 mL Eppendorf tubes and evaporated using centrifugal vacuum concentrators (Labconco CentriVap) at 40 °C for 2 h. The residue was dissolved in 200 μL of solution (acetonitrile: tetrahydrofuran = 7/3 (v/v)). After centrifugation (10,000 g, 5 min), the supernatant was collected for UPLC (Waters ACQUITY) analysis equipped with a Waters FLR detector, a Waters ACQUITY UPLC® BEH C18 column, using 9/1 (v/v) acetonitrile/water containing 0.1% (v/v) trifluoroacetic acid as the mobile phase A and tetrahydrofuran containing 0.1% trifluoroacetic acid as mobile phase B; the A/B = 7/3 (v/v), with 30 °C column temperature and a flow rate of 0.4 mL/min. The eluent was excited with a 540 nm laser and monitored at 590 nm. Standard curves for $PCL_{3.5k}$-RhoB in plasma were generated by the addition of free $PCL_{3.5k}$-RhoB at different concentrations to plasma, followed by extraction and quantification as mentioned above. Pharmacokinetic parameters were obtained using the DAS 3.0 program (BioGuider CO., Shanghai, China).

2.6. Quantitative studies of nanoparticle sccumulation in liver and spleen

Rhodamine B-labeled nanoparticles were administered i.v. into ICR mice at an equivalent dose of 360 μg $PCL_{3.5k}$-RhoB per kg of mouse body weight ($n = 4$ per group). After 1 h, the mice were anesthetized with sodium pentobarbital (2%, 45 mg/kg, Sigma–Aldrich, St. Louis, USA), and the blood was removed by systemic perfusion with PBS containing heparin (300 U/mL). Then the liver and spleen were excised, washed with cold saline, dried on filter paper, weighed and cut into small pieces. The tissues were treated and analyzed using the approach as described in quantitative studies of nanoparticles' accumulation in tumor tissues. To generate the standard curve for $PCL_{3.5k}$-RhoB, the samples were prepared by adding $PCL_{3.5k}$-RhoB with different concentrations in acetonitrile to tissues from untreated mice. The samples were treated and analyzed using the same approach as described above.

2.7. Protein adsorption assay

Rhodamine B-labeled nanoparticles (2 mg/mL, 1 mL) were incubated with 200 μL of murine serum for 1 h at 37 °C. After incubation, nanoparticles were recovered by centrifugation at 14,000 g for 1 h at 4 °C and washed twice with 2 mL cold PBS to remove excess proteins and loosely bound proteins. After the final washing step, the pellets were resuspended in 50 μL lysis buffer containing 2% sodium dodecyl sulfate and 4% triton X-100 to release protein absorbed on the surface of nanoparticles. After another centrifugation (14,000 g, 0.5 h, 4 °C), supernatant was collected and stored at 4 °C. Supernatant (5 μL) was diluted into 100 μL saline, and 25 μL was used to analyze the protein concentration by using the BCA protein assay kit (lot 23250, Thermo, USA), and 20 μL supernatant was loaded into a 4% stacking gel with a 12% resolving gel and subjected to electrophoresis at 120 V for about 60 min. The gels were stained for 20 min using coomassie blue dye (R250, Jinan Pengyuan Biological Technology Co., Ltd., Shandong, China) and washed for one day with bleaching dye (25% ethanol and 8% acetic acid). As a control, 200 μL murine serum was incubated with 1 mL PBS for 1 h at 37 °C, and then the samples were treated and analyzed using the same approach as described above. Blank: As a control, 200 μL murine serum was incubated with 1 mL PBS for 1 h at 37 °C, and then the samples were treated and analyzed using the same approach as described above.

2.8. In vitro cellular uptake

For flow cytometric analysis, MDA-MB-231 cells were seeded into 24-well plates at 8×10^4 cells per well in 0.5 mL of complete DMEM medium at 37 °C in a 5% CO_2 humidified atmosphere for 24 h. The original medium was replaced with Rhodamine B-labeled nanoparticles at an equivalent dose of 90 μg $PCL_{3.5k}$-RhoB per well. The cells were incubated 4 h at 37 °C and were then rinsed twice with cold PBS. The cells were trypsinized, washed twice with cold PBS, and resuspended in cold PBS for flow cytometric analysis using a BD FACSCalibur flow cytometer.

For microscopic observation, MDA-MB-231 cells (2×10^4 cells/well) were seeded on coverslips in a 24-well plate and incubated for 24 h. The original medium was replaced with Rhodamine B-labeled nanoparticles at an equivalent dose of 90 μg $PCL_{3.5k}$-RhoB per well. The cells were incubated for 4 h at 37 °C and were then rinsed twice with cold PBS and fixed with 4% formaldehyde for 10 min at room temperature. The cells were stained with Alexafluor 488 phalloidin (Invitrogen, Carlsbad, CA) to indicate the cytoskeleton, and counterstained with DAPI (Sigma–Aldrich, St. Louis, USA) to indicate cell nuclei according to the standard protocol provided by the suppliers. Coverslips were mounting media (Sigma–Aldrich, St. Louis, USA) to reduce fluorescent photobleaching. The cellular uptake of nanoparticles was visualized by CLSM (LSM 710, Carl ZeissInc., Jena, Germany).

For quantitative analysis, RAW264.7 cells or MDA-MB-231 cells were seeded into 24-well plates at 8×10^4 cells per well, in 0.5 mL of complete RPMI-1640 or DMEM medium at 37 °C, in a 5% CO_2

humidified atmosphere for 24 h. The original medium was replaced with Rhodamine B-labeled nanoparticles at an equivalent dose of 90 μg $PCL_{3.5k}$-RhoB per well. The cells were incubated for 4 h at 37 °C and were then rinsed twice with cold PBS. The cells were trypsinized, washed twice with cold PBS, and resuspended in 100 μL lysis buffer containing 2% SDS and 4% triton X-100. 500 μL of acetonitrile was added to precipitate proteins. After centrifugation (5000 g, 5 min), the supernatant was collected for UPLC analysis.

2.9. Quantitative studies of nanoparticles accumulation in tumor tissue

Rhodamine B-labeled nanoparticles were administrated intravenously into BALB/c nude mice bearing MDA-MB-231 tumors, at an equivalent dose of 360 μg $PCL_{3.5k}$-RhoB per kg of mouse body weight (n = 4 for each group). After a predetermined time (6, 12, 24 h), tumor tissues were excised, washed with cold saline, dried over filter paper, weighed, cut into small pieces and put into 2 mL FastPrep® lysing matrix tubes with five stainless steel beads (2 mm), to which 500 μL acetonitrile was added. The tissue was then homogenized with a FastPrep system with a speed of 4 m/s for 40 s. The lysis buffer was further extracted with 1 mL chloroform by vortex mixing for 10 s. After centrifugation (10,000 g, 5 min), the organic phase was separated into 2.0 mL Eppendorf tubes and evaporated using centrifugal vacuum concentrators (Labconco CentriVap) at 40 °C for 2 h. The residue was dissolved in 200 μL of solution (acetonitrile: tetrahydrofuran = 7/3 (v/v)). After centrifugation (10,000 g, 5 min), the supernatant was collected for UPLC analysis. To generate the standard curve for $PCL_{3.5k}$-RhoB, the samples were prepared by adding $PCL_{3.5k}$-RhoB with different concentrations in acetonitrile to tumor tissue from untreated mice. The samples were treated and analyzed using the same approach as described above.

2.10. In vivo tumor cellular uptake

Rhodamine B-labeled nanoparticles were intravenously administered into BALB/c nude mice bearing an MDA-MB-231-GFP breast cancer xenograft at an equivalent dose of 360 μg $PCL_{3.5k}$-RhoB per kg of mouse body weight (n = 4 for each group). The mice were euthanized 12 h later and tumor tissues were collected. Tumor tissues were transferred to a dish and cut into small pieces. Then the pelleted materials were resuspended with 10 mL tumor cell digestion solution (1 mg/mL collagenase I, Invitrogen, Carlsbad, CA) and incubated at 37 °C for 2 h with agitation. Tumor cells were then collected by centrifugation at 1200 g for 5 min at 4 °C and washed twice with PBS containing 1% fetal bovine serum (FBS, ExCell Bio, Shanghai, China). Tumor cells were filtered through a 200-mesh sieve and sorted on a BD FACSAria Cell Sorter. The amplification scale was logarithmic for FL1-H parameters, and linear for SSC-H and FSC-H. GFP-expressing MDA-MB-231 tumor cells were carefully gated out using FL1-H versus SSC-H bivariant graphs. Then the tumor cells (10^7 cells) were collected and treated with the method as above and analyzed by UPLC.

2.11. Inhibition of tumor growth

When the tumor volume of the MDA-MB-231 xenograft was around 60 mm^3 on the 15th day after implantation, the mice were randomly divided into nine groups (five mice per group) and treated with PBS, Taxol®, NP_{blank} (nanoparticles component of $PEG_{3.4k}$—$PCL_{3.7k}$/$PCL_{3.5k}$), or DTXL-loaded nanoparticles with different surface PEG densities at an equivalent dose of 2 mg DTXL per kg of mouse body weight by intravenous injection. The dose of NP_{blank} was 75 mg nanoparticles/kg. The mice received injections every other day. Tumor growth was monitored by measuring the perpendicular diameter of the tumor using calipers. The estimated volume was calculated according to the following equation: tumor volume (mm^3) = 0.5 × length × $width^2$. Mouse body weight was also monitored after administration every other day. Twenty four hours after the last injection, mice were euthanized and the tumors were taken out for images and weighing.

For the survival study, 4 days after implantation of murine melanoma cell line B16 into C57BL/6 mice, mice were randomly divided into nine groups (ten mice per group) and i.v. injected with PBS, Taxol®, NP_{blank} and DTXL-loaded nanoparticles with varying surface PEG densities. The dose of DTXL and NP_{blank} was 3 mg/kg and 110 mg/kg, respectively. Treatment was repeated every other day ten times and mice were checked for survival every day.

2.12. Statistical analysis

The statistical significance of treatment outcomes was assessed using Student's t-test (two-tailed); $p < 0.05$ was considered statistically significant in all analyses (95% confidence level).

3. Results and discussion

3.1. Regulation of surface PEG density and size of polymeric nanoparticles

Amphiphilic block copolymers can self-assemble into nanoscale particles in aqueous solution as a result of energetic repulsion effects between blocks [35]. The structural performance of the assembly is influenced by its composition of the polymer, the lengths of the block segments, the dispersion solvent selected initially and so on [36]. We assumed that the surface PEG density of assembly could be changed by incorporating hydrophobic homopolymer into the relative amphiphilic polymers during preparation of nanoparticles, which alters the micelle aggregation number and increases the core volume of assembly. In the experiments, we firstly chose $PEG_{3.4k}$—$PCL_{3.7k}$ block copolymer with the number-average molecular weights of 3.4 k and 3.7 k respectively, and incorporated $PCL_{3.5k}$ (PCL homopolymer with a number-average molecular weight of 3.5 k) at different mass ratios, then polymeric nanoparticles were obtained by a method of solvent exchanging, in which there is sufficient time for the self-assembly to reach equilibrium [36,37]. The surface PEG density of nanoparticles obtained can be changed controllably by varying the incorporated proportion of PCL homopolymer and increasing the volume of the assembly (Fig. 1A). As shown in Fig. 1B, when the molar ratio of CL from $PCL_{3.5k}$ homopolymer and $PEG_{3.4k}$—$PCL_{3.7k}$ copolymer to EG from $PEG_{3.4k}$—$PCL_{3.7k}$ copolymer in the mixture increased from 0.46 to 1.06, the volume of assembly was raised nearly linearly from 1.2×10^5 to 15.4×10^5 nm^3. Correspondingly, the mean hydrodynamic diameter increased from 62 nm to 143 nm, which was also confirmed by transmission electron microscopy (TEM) observations (Fig. 1C). While the PEG content inevitably decreased from 46% to 27% with the addition of PCL homopolymer and increase of nanoparticles' size, this might lead to a change in the surface PEG density. As measured by static light scattering (SLS), the average molecular weight of an individual nanoparticle ($M_{W(NP)}$) was obtained, then the core radius (R_C) of an individual assembly was calculated by Equation (1), where the K_1 was the weight ratio of PCL in nanoparticles, the core density (ρ_C) of micelle was 1.146 g/cm^3 and N_A denoted the Avogadro constant. The number of PEG—PCL chains (N) in a single nanoparticle was calculated by Equation (2), where the K_2 represented the weight ratio of PEG—PCL in nanoparticles and $M_{W(PEG-PCL)}$ represented the average number molecular weight of PEG—PCL block copolymer. Then the surface PEG density (σ) was defined by Equation (3). In these calculations, it was

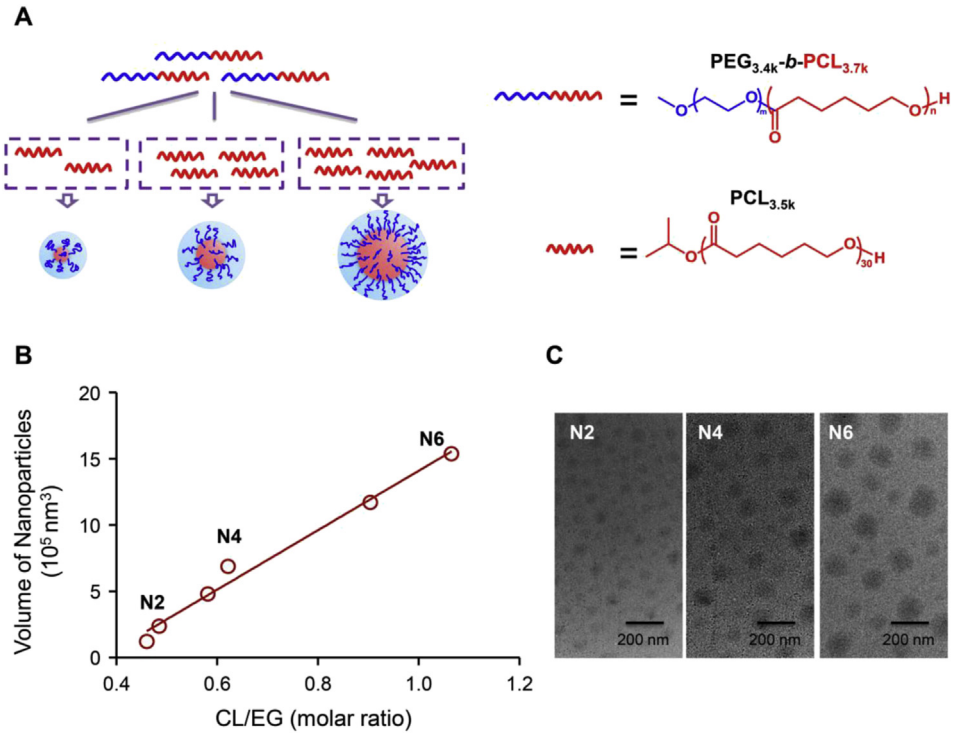

Fig. 1. Regulation of the diameter of polymeric nanoparticles. (A) Schematic showing the increase in the diameter of polymeric nanoparticles as the content of $PCL_{3.5k}$ homopolymer increased during the preparations. In the nanoparticles, PCL forms the core through hydrophobic interactions (red), PEG forms the corona (blue) and the sky-blue represents the hydration layer on nanoparticles. (B) The increase in volume of the polymeric nanoparticles was dependent on the ratios of CL from PCL homopolymer and PEG–PCL copolymer to EG from PEG–PCL in the mixture, in a nearly linear fit. ($R^2 = 0.9845$) (C) TEM images of nanoparticles chosen in B, which had a hydrodynamic-diameter of 62, 110 and 143 nm, respectively. (For interpretation of the references to color in this figure legend, the reader is referred to the web version of this article.)

assumed that PEG presented a uniform layer on the surface of the nanoparticles. As shown in Table 1, as the ratio of CL to EG increased, the core radius (R_C) of nanoparticles grew from 9.8 to 44.6 nm, and the PEG density increased from 0.56 to 1.10 PEG/nm^2, which indicated that the surface PEG densities of assembly were controlled by the addition of hydrophobic homopolymer at different mass ratios into the corresponding amphiphilic copolymer.

$$M_{W(NP)} \times K_1 = \rho_C \times \frac{4}{3}\pi R_C^3 \times N_A \quad (1)$$

$$N = M_W \times K_2 \Big/ M_{W(PEG-PCL)} \quad (2)$$

$$\sigma = N \Big/ 4\pi R_C^2 \quad (3)$$

3.2. Preparation of polymeric nanoparticles with varied surface PEG density but similar size

A variety of properties of nanoparticles could significantly affect their biological behaviors [23]. In order to study more precisely the influence of surface PEG densities on the in vivo fate of nanoparticles, the other characteristics of nanoparticles used in this study should be kept as constant as possible; that is, the particles' size should also be kept basically the same while the PEG density changes. Since the size of nanoparticles will also change with the varying molecular weight of the PCL block in PEG–PCL [38], it is assumed that a library of nanoparticles with different sizes and PEG

Table 1
Parameters calculated for determining the surface PEG density.

Name	$PCL_{3.5k}/PEG_{3.4k}$–$PCL_{3.7k}$ (PCL_{31}/PEG_{77}-PCL_{32})[a]		CL/EG[c] (molar ratio)	Rc[d] (nm)	N[e]	σ[f] (PEG/nm^2)
	Wt/Wt[b]	Molar ratio				
N1	0.05	0.10	0.46	9.8	673	0.56
N2	0.08	0.16	0.48	12.3	1245	0.66
N3	0.20	0.41	0.58	17.8	3164	0.86
N4	0.25	0.51	0.62	21.3	5115	0.90
N5	0.60	1.22	0.90	36.3	17,298	1.05
N6	0.80	1.62	1.06	44.6	27,410	1.10

[a] PCL_{31} means the repeat units for CL in PCL is 31. PEG_{77}–PCL_{32} means the repeat units for EG and CL is 77 and 32 respectively.
[b] Weight ratio (Wt/Wt) of $PCL_{3.5k}$ homopolymer to $PEG_{3.4k}$–$PCL_{3.7k}$ copolymer.
[c] Repeat units of PCL (CL) and PEG (EG).
[d] The core radius (R_C) of an individual nanoparticle.
[e] The number of PEG–PCL chains (N) in a single nanoparticle.
[f] PEG density on surface of a nanoparticle, calculated from static light scattering measurements.

densities could be obtained by synthesizing a series of PEG–PCL copolymers with an unchanged PEG block molecular weight while gradually increasing the PCL block molecular weight, and preparing the nanoparticles using the same method as described above. Then a group of nanoparticles with varying PEG density and similar hydrodynamic diameter could be picked from the library for further study (Fig. 2A). The result shown in Fig. 2B demonstrated similarly that the volumes of nanoparticles changed nearly linearly depending on the ratios of CL to EG for an identical PEG–PCL copolymer. Nanoparticles with a mean hydrodynamic diameter of 100 ± 10 nm with polydispersity indices (PDI) below 0.2 in this library were chosen for further analysis of their surface PEG density. The size distribution and morphology was confirmed by DLS and TEM (Figs. S1 and S2). These nanoparticles display similar zeta potentials, ranging from −4.7 to −2.1 mV at pH 7.4 in water. The ^{1}H NMR of these nanoparticles in $CDCl_3$ after lyophilized shows that more than 96% of PCL homopolymers were integrated in the nanoparticles (data not show).

The surface PEG density of nanoparticles was quantified by SLS detection combined with calculations as described above. As shown in Table 2, the surface PEG density was affected by the molecular weight of PEG–PCL and inputted ratios of CL to EG, and gradually declined from 0.86 to 0.19 PEG/nm^2 as the molecular weight of the PCL block in PEG–PCL increased from 3.7 k to 12.0 k while the average hydrodynamic nanoparticles size was kept at ~100 nm. The conformation of the PEG chains on the surface of nanoparticles is further described by the relationship between D (the distance between neighboring PEG graft sites), L (the length of the PEG chain on the surface of the nanoparticle) and RF (Flory radius, dependent on the PEG molecular weight), and defined as "dense brush" ($L > 2R_F$), "brush" ($D < R_F$) or "mushroom" ($D > R_F$) [8,17,39,40]. According to calculations described in the supporting information, at low PEG densities (0.19–0.36 PEG/nm^2), PEG chains adopt a "brush" conformation; when PEG density is higher than 0.55 PEG/nm^2, PEG chains arrange in a "dense brush" regime. Herein, we obtained nanoparticles with varied surface PEG densities but similar particle size in order to further study the impact of surface PEG density on the in vivo fate of nanoparticles.

3.3. Nanoparticles with high surface PEG density exhibited a remarkably long circulation

Previous reports revealed that "stealth" behavior of nanoparticles can be induced by PEGylation, and is often critically dependent on their surface PEG density and conformation [2,41,42]. We then evaluated how the pharmacokinetics of nanoparticles changes over a range of surface PEG densities all in a brush regime. In order to quantify nanoparticles in plasma, $PCL_{3.5k}$-RhoB, a conjugate of Rhodamine B to $PCL_{3.5k}$, was used to replace part of $PCL_{3.5k}$ when nanoparticles were prepared. The Rhodamine B-labeled nanoparticles with different PEG densities and same sizes were injected intravenously into ICR mice. After appropriate times, blood was collected for analysis of remaining nanoparticles in plasma. The blood clearance curves are shown in Fig. 3 and the pharmacokinetic parameters were analyzed in a non-compartment model. Although the PEG chains were present in a brush regime, nanoparticles with a lower PEG density of 0.19 and 0.25 PEG/nm^2 were quickly cleared from the blood (Fig. 3A). In contrast, nanoparticles with a higher PEG density than 0.36 PEG/nm^2 exhibited a remarkably long circulation. It was seen that the concentration of nanoparticles in blood remained high after 48 h. The area under the plasma concentration–time curve ($AUC_{(0-48\ h)}$) for nanoparticles with a surface PEG density of 0.36 PEG/nm^2 was 12.3-fold and 104.5-fold larger than for those with a lower PEG density of 0.25 and 0.19 PEG/nm^2, respectively (Fig. 3B). As the surface PEG density of nanoparticles increased into a "dense brush" regime, the surface PEG density increased accordingly, resulting in a continually increasing $AUC_{(0-48\ h)}$. Clearance (CL_Z) of nanoparticles was significantly decreased as their surface PEG density increased (Fig. 3C). Meanwhile, the terminal half-life ($T_{1/2}$, another parameters important in drug delivery applications) of nanoparticles with a higher surface PEG density of 0.86 PEG/nm^2 increased to 17.069 ± 1.826 h, compared to nanoparticles with a lower PEG density of 0.19 PEG/nm^2 (0.267 ± 0.067 h) (Fig. 3D). These results indicated that nanoparticles' pharmacokinetics are greatly relative to their surface PEG density, and that even with a high PEG density in a "dense brush" regime, prolonged blood circulation appeared to need a higher PEG density. Meanwhile, it is worth noting that nanoparticles' diameters can be maintained unchanged in serum-contained conditions for over 48 h at 37 °C (Fig. S3).

It is well established that the blood clearance is facilitated by the accumulation in the mononuclear phagocyte system (MPS) [43]. Therefore, the liver and spleen organs were resected after tail vein injection of nanoparticles and analyzed to determine whether MPS organs accumulation was also dependent on PEG coating density. As shown in Fig. 4A and B, accumulations of nanoparticles in the liver and spleen were high for nanoparticles with lower surface PEG densities. As surface PEG density

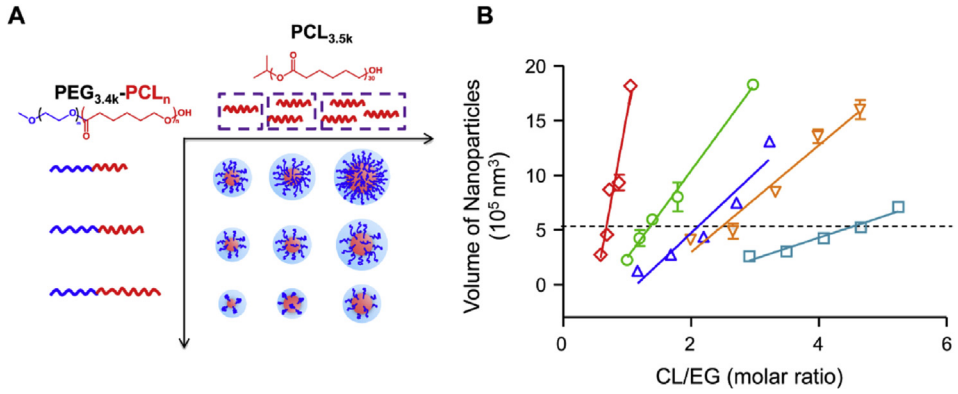

Fig. 2. Preparation of polymeric nanoparticles with varied surface PEG densities and diameters. (A) Illustration of a library of nanoparticles could be obtained by changing the PCL block of PEG–PCL and the content of PCL homopolymer incorporated. (B) The increase in volume of the nanoparticles was dependent on the ratios of CL to EG in a nearly-linear fit for an identical PEG–PCL copolymer (Red line: $PEG_{3.4k}$–$PCL_{4.5k}$/$PCL_{3.5k}$; Green line: $PEG_{3.4k}$–$PCL_{5.3k}$/$PCL_{3.5k}$; Blue line: $PEG_{3.4k}$–$PCL_{5.7k}$/$PCL_{3.5k}$; Orange line: $PEG_{3.4k}$–$PCL_{8.3k}$/$PCL_{3.5k}$; Light blue line: $PEG_{3.4k}$–PCL_{12k}/$PCL_{3.5k}$). The dotted line represents the volume of nanoparticles with the hydrodynamic diameters of 100 nm, and nanoparticles around the line were selected for further study. (n = 3, date are means ± SD.) (For interpretation of the references to color in this figure legend, the reader is referred to the web version of this article.)

Table 2
PEG density and conformation on surface of nanoparticles.

Formulation	Composition				CL/EG (molar ratio)	R_h[b] (nm)	R_F[c] (nm)	D[d] (nm)	L[e] (nm)	PEG density (PEG/nm^2)	Regime
	PEG-PCL	PCL	PCL/PEG–PCL (W_t/W_t)	PCL/PEG–PCL (molar ratio)							
$ND_{0.86}$[a]	$PEG_{3.4k}$–$PCL_{3.7k}$ (PEG_{77}–PCL_{32})	$PCL_{3.5k}$ (PCL_{31})	0.20	0.41	0.58	103 ± 5.5	4.7	1.22	11.73	0.86	Dense brush
$ND_{0.72}$[a]	$PEG_{3.4k}$–$PCL_{4.5k}$ (PEG_{77}–PCL_{39})	$PCL_{3.5k}$ (PCL_{31})	0.19	0.43	0.68	96 ± 0.9	4.7	1.33	11.07	0.72	Dense brush
$ND_{0.55}$[a]	$PEG_{3.4k}$–$PCL_{5.3k}$ (PEG_{77}–PCL_{46})	$PCL_{3.5k}$ (PCL_{31})	0.70	1.74	1.29	104 ± 1.3	4.7	1.56	9.97	0.55	Dense brush
$ND_{0.36}$[a]	$PEG_{3.4k}$–$PCL_{5.7k}$ (PEG_{77}–PCL_{50})	$PCL_{3.5k}$ (PCL_{31})	1.50	3.90	2.20	94 ± 1.3	4.7	1.89	8.76	0.36	brush
$ND_{0.25}$[a]	$PEG_{3.4k}$–$PCL_{8.3k}$ (PEG_{77}–PCL_{73})	$PCL_{3.5k}$ (PCL_{31})	1.27	4.25	2.66	98 ± 4.6	4.7	2.27	7.75	0.25	brush
$ND_{0.19}$[a]	$PEG_{3.4k}$–$PCL_{12.0k}$ (PEG_{77}–PCL_{105})	$PCL_{3.5k}$ (PCL_{31})	1.85	8.14	4.66	96 ± 1.4	4.7	2.60	7.08	0.19	brush

[a] Nanoparticles with different surface PEG density. For example: $ND_{0.86}$ means nanoparticles with the surface PEG density at 0.86 PEG/nm^2.
[b] Hydrodynamic diameters (R_h) measured by dynamic light scattering (DLS).
[c] Flory radius (R_F), dependent on the PEG molecular weight.
[d] The distance (D) between neighboring PEG chain on the surface of the nanoparticle.
[e] The length of the PEG chain (L) on the surface of the nanoparticle.

increased, the contents of nanoparticles in these organs decreased significantly. Moreover, when a dense brush conformation was presented on the nanoparticles, only a small decrease was observed in the liver and spleen, which was consistent with the trends of pharmacokinetics parameters. To further clarify the in vivo behaviors of nanoparticles with different surface PEG densities, we conducted in vitro the serum protein binding and macrophage uptake of nanoparticles. Total protein adsorptions on the surface of nanoparticles measured by bicinchoninic (BCA) assay were presented in Fig. S4, and protein isolates from nanoparticles were further analyzed by polyacrylamide gel electrophoresis (PAGE) (Fig. 4C). Nanoparticles with the lowest surface PEG density at 0.19 PEG/nm^2 interacted strongly with serum proteins, and increasing PEG density from 0.19 to 0.36 PEG/nm^2 significantly reduced the total serum protein adsorption. However, when the surface PEG density was higher than 0.55 PEG/nm^2, which presented as a dense brush conformation, the serum protein adsorption decreased negligibly when PEG density was further increased, indicating that nanoparticles with surface PEG density in a dense brush regime effectively prevented the serum protein adsorption. To address macrophage uptake, Rhodamine B-labeled nanoparticles were incubated with RAW264.7 cells in cell culture medium. Macrophage uptake presented in a PEG density-dependent manner (Fig. 4D). These results indicated that an increase in surface PEG density leads to decreased serum protein adsorption and prolonged blood circulation time.

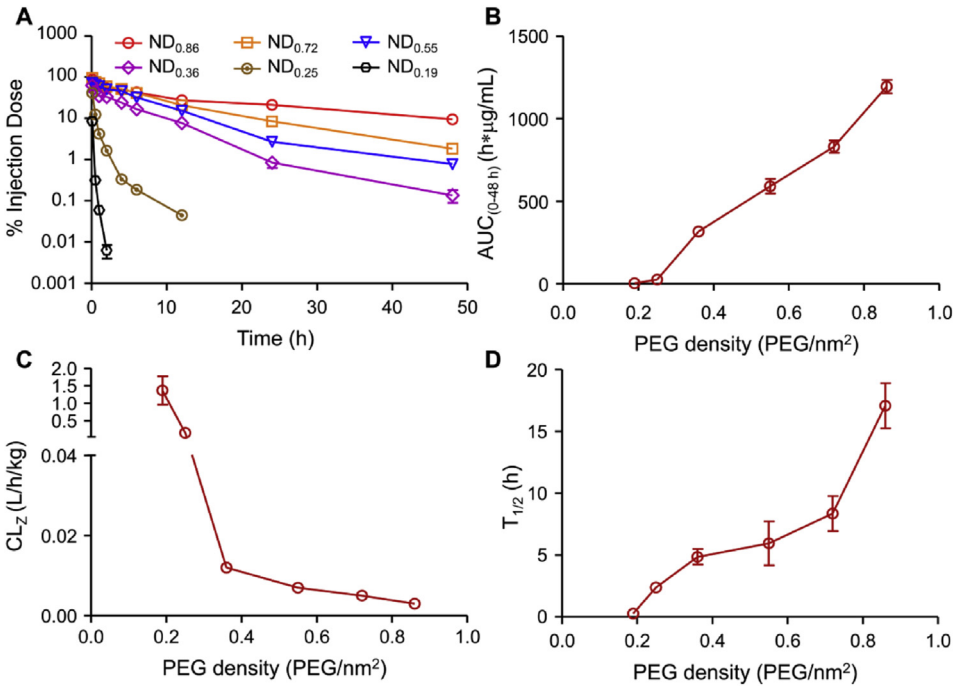

Fig. 3. Influence of surface PEG densities on the pharmacokinetics parameters. (A) Concentration–time curve of nanoparticles with varying PEG densities in mice plasma after i.v. administration (n = 4). Area under the plasma concentration–time curve ($AUC_{(0-48\ h)}$) (B), clearance (CL_Z) (C) and terminal half-time ($T_{1/2}$) (D) pharmacokinetics parameters were analyzed in a non-compartment model. (n = 4, data are means ± SD.)

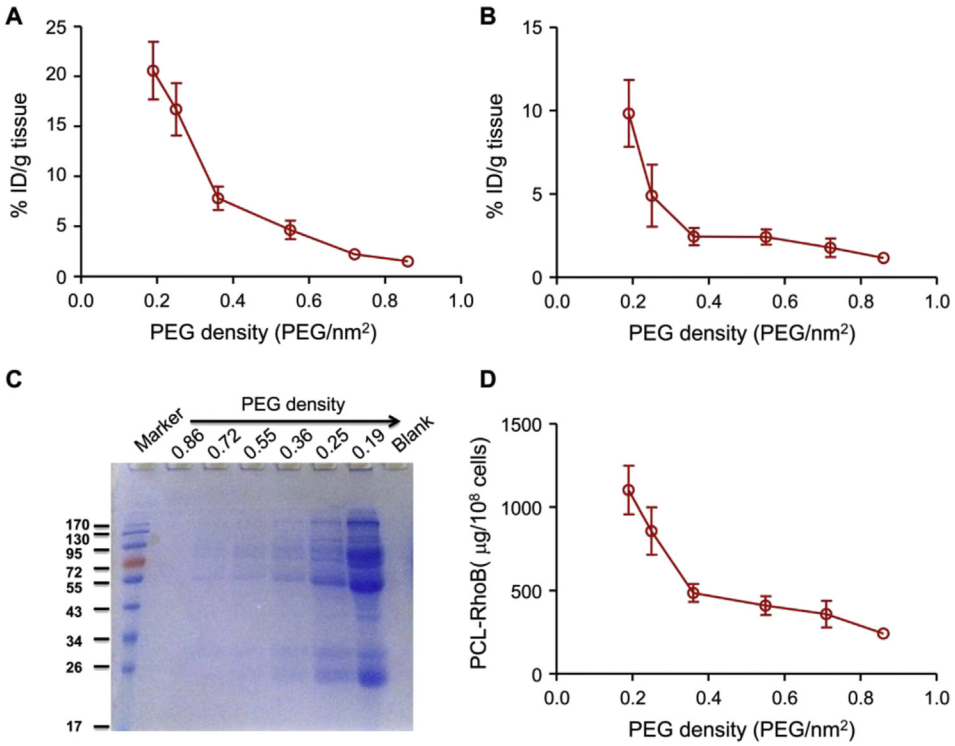

Fig. 4. Distribution of nanoparticles with different surface PEG densities in liver (A) and spleen (B). (n = 4, data are means ± SD) (C) Qualitative analysis for serum protein adsorbed on nanoparticles with varying PEG densities by sodium dodecyl sulfate polyacrylamide gel electrophoresis (SDS-PAGE). (D) Macrophage uptake of nanoparticles. (n = 4, data are means ± SD).

3.4. Higher surface PEG density assists more nanoparticles accumulated in tumor tissue, compensating for the defect of decreased uptake by tumor cells

It was hypothesized that nanoparticles with longer circulation times allow a greater chance to accumulate in the tumor tissue by the enhanced permeability and retention effect (EPR effect) [44–46]. We then evaluated the content of nanoparticles in tumors following intravenous injection of nanoparticles into nude mice bearing MDA-MB-231 xenografts, to investigate whether it could enhance the accumulation of nanoparticles to a greater degree in tumor tissue by increasing PEG density. As shown in Fig. 5, nanoparticles with higher PEG density accumulated more easily in tumors, which may have occurred due to the prolonged circulation time. Nanoparticles with the highest surface PEG density showed 208-fold, 150-fold and 66-fold higher accumulation in tumor tissues compared to nanoparticles with the lowest PEG density at 6, 12 and 24 h, respectively.

Accumulation of nanoparticles in tumor provided opportunities for uptake by tumor cells. However, even though PEGylation minimizes the nonspecific interactions of nanoparticles with serum components, thus potentially extending the blood circulation of nanoparticles and improving accumulation in the tumor following intravenous administration, previous studies unfortunately showed that PEGylation also markedly reduces nanoparticles' cellular uptake in all cells non-specifically as well as in tumor cells, limiting their antitumor efficiency in vivo [47–51]. We firstly examined in cell culture the influence of surface PEG density on cellular uptake in tumor cells. MDA-MB-231 cells were incubated with Rhodamine B-labeled nanoparticles for 4 h at 37 °C in cell culture medium. As observed with confocal laser scanning microscopy, cells treated with nanoparticles with lower surface PEG density showed enhanced intracellular fluorescence signals (Fig. 6A). The result was also corroborated by flow cytometric analysis (Fig. 6B and C). To further precisely quantitatively analyze the cellular fluorescence, cells after treatment were collected and $PCL_{3.5k}$-RhoB was extracted for UPLC analysis. As shown in Fig. 6D, nanoparticles with the lowest surface PEG density exhibited the strongest cellular uptake compared with those with a higher surface PEG density. Increasing the PEG density led to weaker cellular uptake, which was consistent with the findings of other studies [18,52]. These results clearly demonstrated that the reduction in the cellular uptake of nanoparticles by tumor cells is dependent on surface PEG density.

The cellular uptake of nanoparticles by tumor cells in vivo was always affected by other factors. We next examined the cellular uptake of nanoparticles in vivo by tumor cells. Rhodamine B-labeled nanoparticles were injected intravenously in mice bearing

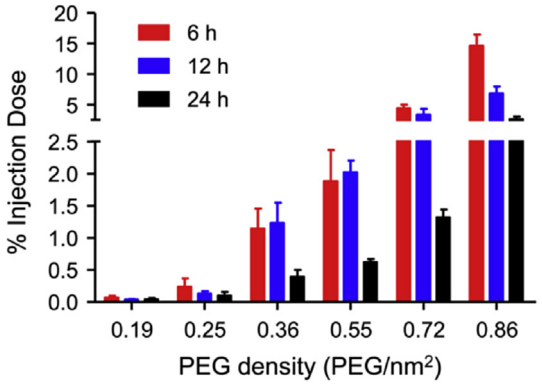

Fig. 5. Accumulations of nanoparticles with different surface PEG densities in tumor tissue after 6, 12 or 24 h injection. (n = 4, data are means ± SD).

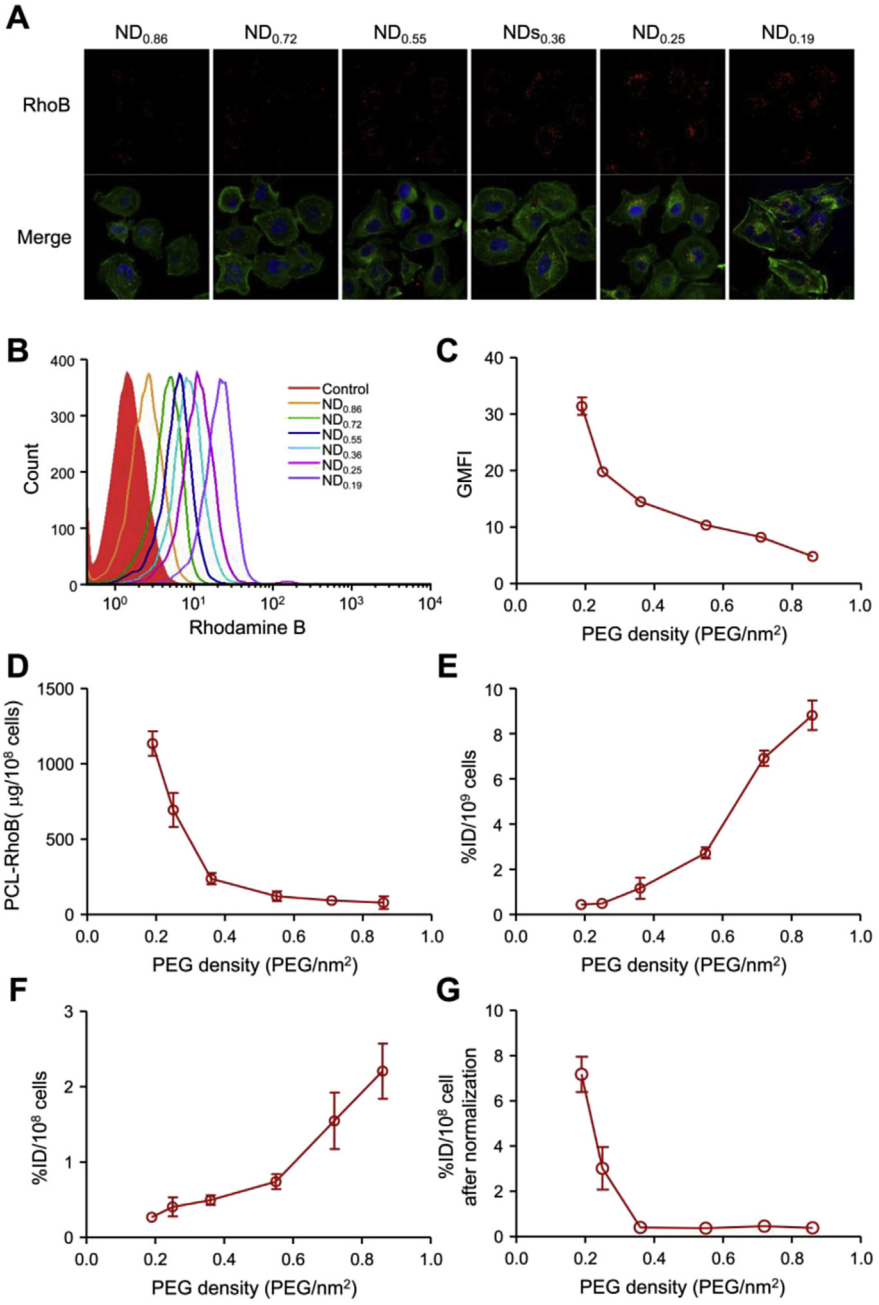

Fig. 6. Surface PEG density affects the cellular uptake of nanoparticles by tumor cells. (A) Internalization of nanoparticles observed by confocal laser scanning microscopy. Red represents nanoparticles labeled with Rhodamine B; green and blue are cell cytoskeleton F-actin and cell nuclei counterstained by Alexa Fluor 488 phalloidin and DAPI, respectively. (B and C) Flow cytometric analyses of MDA-MB-231 cells after 4 h incubation with Rhodamine B-labeled nanoparticles with different PEG densities (B) and quantification of cell internalization shown as mean fluorescence intensity (MFI) (C). (D) Quantification analysis of cell internalization of nanoparticles in cell culture by MDA-MB-231 cells. (E and F) Cellular uptake of nanoparticles by total cells from tumor tissue (E) and GFP-expressing tumor cells in tumor tissue (F). (n = 4, data are means ± SD) (G) Cellular uptake by GFP-expressing tumor cells in tumor after normalization to the amount of nanoparticles accumulated in tumor at the same time point of 12 h. (For interpretation of the references to color in this figure legend, the reader is referred to the web version of this article.)

GFP-expressing MDA-MB-231 tumors, and after 12 h, the tumor was excised, dispersed into single cells, and Rhodamine B-labeled nanoparticles taken up by 10^7 cells from the tumor tissue were quantitatively analyzed. As shown in Fig. 6E, nanoparticles with higher surface PEG density demonstrated a higher cellular uptake by cells from tumor tissue. To further investigate whether nanoparticles accumulated in tumor tissue could be internalized efficiently by tumor cells, we isolated the GFP-expressing tumor cells that occupy about 25% of all cells from tumor tissue, and further analyzed the quantity of nanoparticles in the GFP-expressing tumor cells. As shown in Fig. 6F, though nanoparticles with the lowest PEG density had the largest uptake by tumor cells in vitro, the nanoparticles were present in the GFP-expressing MDA-MB-231 cells in vivo at the lowest value, which should be caused by the shortest blood circulation and poorest accumulation in tumor tissue. As the PEG density increased, an enhanced enrichment of nanoparticles in GFP-expressing tumor cells was observed, suggesting that the contents of nanoparticles in tumor cells in vivo is a consolidated

result of blood circulation, tumor accumulation and cellular uptake. However, when the cellular uptake of nanoparticles by GFP-expressing tumor cells in vivo to tumor accumulation was normalized, it still exhibited a relatively higher cellular uptake of nanoparticles with lower surface PEG density (Fig. 6G). This result is consistent with that in the cell culture medium, indicating that higher surface PEG density assists, to some extent, the enrichment of more nanoparticles in tumor tissue, compensating for the defect of decreased uptake by tumor cells.

3.5. Higher surface PEG density enriches nanoparticles in tumor cells in vivo, exhibiting higher antitumor efficacy

The antitumor activities are the comprehensive effect of "blood circulation," "tumor accumulation," "cellular uptake" and so on, due to the tortuous journey of nanomedicines from their site of introduction to their molecular site of action. In an attempt to demonstrate this, docetaxel (DXTL) was used as the model drug to explore the anti-tumor effect of nanoparticles with varying surface PEG densities on tumor growth inhibition of MDA-MB-231 breast cancer, and was also used in a survival study of B16 melanoma following intravenous administration.

In the MDA-MB-231 model, all of the DTXL-loaded nanoparticles with varying surface PEG densities were effective in retarding tumor growth compared to the treatment with PBS (Fig. 7A and Fig. S5A). Administration of DTXL-loaded nanoparticles with the lowest surface PEG density (0.19 PEG/nm^2) presented a weak effect on tumor growth inhibition, similar to the treatment of Taxol®, with tumor growth inhibition rates of 41.0% and 40.8%, respectively. Increasing the surface PEG density of nanoparticles efficiently enhanced the antitumor activities, and the tumor inhibition ratio was 91.5% in the $ND_{0.86}$ group. The weight of the tumor mass after treatments (Fig. 7B and Fig. S5B) exhibited similar trends, and no significant body weight loss was observed in any of the treated mice (Fig. S5C).

The anti-tumor therapy was also conducted in the B16 melanoma model. The survival curves were examined and presented in Fig. 7C. Mice treated with DTXL-loaded nanoparticles showed a significant increase in life span compared to the PBS treatment. Increasing the surface PEG density of nanoparticles could further extend the survival time. Administration of Taxol® resulted in only a slight extended survival time of mice. Drug-free nanoparticles presented no effect on mice survival compared with PBS (Fig. S5D). These in vivo and in vitro data confirm that nanoparticles with higher surface PEG density could deliver more drugs to tumor cells following systemic administration, resulting in significantly enhanced antitumor activities.

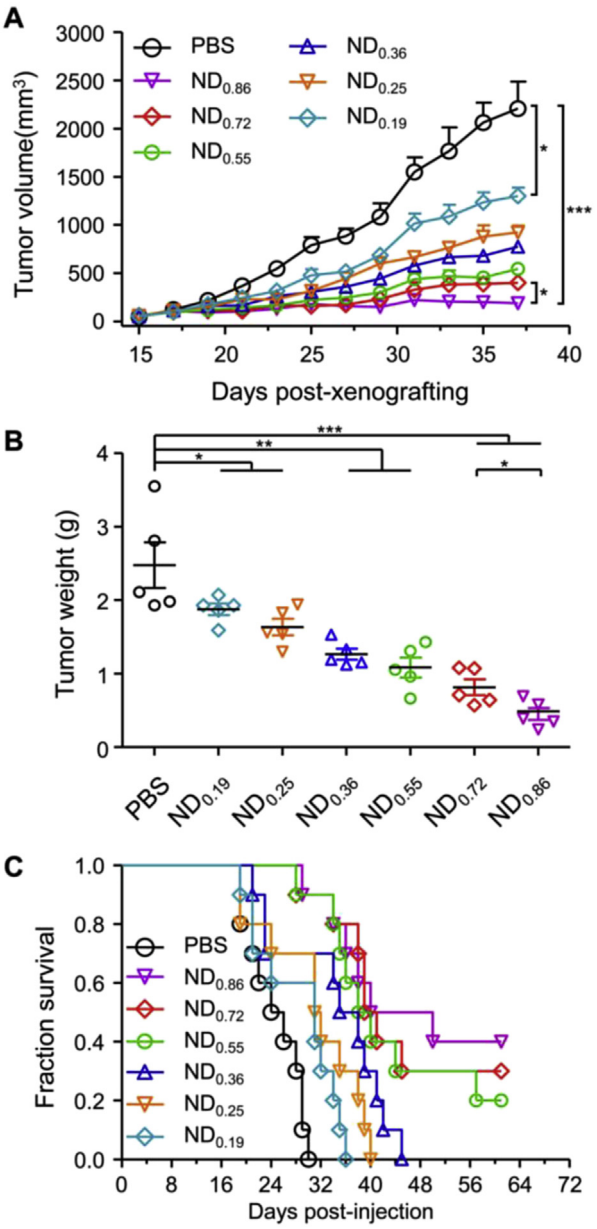

Fig. 7. Antitumor activities of DTXL-loaded nanoparticles with different surface PEG densities. (A) Efficacy of DTXL-loaded nanoparticles with varying surface PEG densities on MDA-MB-231 tumor growth inhibition. (n = 5, data are means ± SD) (B) Tumor weight after the last treatment to MDA-MB-231 tumor-bearing mice. (C) Survival curves of B12 tumor bearing mice. *p < 0.05, **p < 0.01, ***p < 0.001.

4. Conclusions

We regulated the polymeric nanoparticles' size and surface PEG density, using a highly tunable method by incorporating PCL homopolymer into PEG–PCL copolymer and adjusting the ratio of these components. The increase in the volume of nanoparticles was nearly linearly dependent on the molar ratio of CL/EG. The surface PEG density also increased significantly with the gradual increase of the molar ratio of CL/EG. By changing the molecular weight of the PCL block in PEG–PCL, a library of nanoparticles with different sizes and surface PEG densities was established. A group of nanoparticles with similar sizes around 100 nm and varying surface PEG densities were selected for further studying the influence of surface PEG density on nanoparticles' behaviors, both in vitro and in vivo. As in the surface PEG density increased, it resulted in a conformation change from "brush" to "dense brush," showing significant improvements in the nanoparticles' pharmacokinetics and accumulation in tumor tissue. Although it was observed that nanoparticles with a lower surface PEG density had a higher cellular internalization in tumor cells in vitro, more nanoparticles with a higher surface PEG density accumulated in GFP-expressing tumor cells in vivo, leading to advanced anti-tumor activities.

Acknowledgments

Thanks to the support of Core Facility Center for Life Sciences, University of Science and Technology of China. This work was supported by the National Basic Research Program of China (973 Programs, 2012CB932500, 2015CB932100 and 2013CB933900), and the National Natural Science Foundation of China (51125012, 51390482), and the Fundamental Research Funds for the Central Universities.

Appendix A. Supplementary data

Supplementary data related to this article can be found at http://dx.doi.org/10.1016/j.biomaterials.2015.07.048.

References

[1] J.A. Hubbell, A. Chilkoti, Nanomaterials for drug delivery, Science 337 (2012) 303–305.
[2] F.M. Veronese, G. Pasut, PEGylation, successful approach to drug delivery, Drug Discov. Today 10 (2005) 1451–1458.
[3] Q. Dai, C. Walkey, W.C.W. Chan, Polyethylene glycol backfilling mitigates the negative impact of the protein corona on nanoparticle cell targeting, Angew. Chem. Int. Ed. 53 (2014) 5093–5096.
[4] K. Knop, R. Hoogenboom, D. Fischer, U.S. Schubert, Poly(ethylene glycol) in drug delivery: pros and cons as well as potential alternatives, Angew. Chem. Int. Ed. 49 (2010) 6288–6308.
[5] A. Gabizon, R. Catane, B. Uziely, B. Kaufman, T. Safra, R. Cohen, et al., Prolonged circulation time and enhanced accumulation in malignant exudates of doxorubicin encapsulated in polyethylene-glycol coated liposomes, Cancer Res. 54 (1994) 987–992.
[6] W.T. Lim, E.H. Tan, C.K. Toh, S.W. Hee, S.S. Leong, P.C. Ang, et al., Phase I pharmacokinetic study of a weekly liposomal paclitaxel formulation (Genexol-PM) in patients with solid tumors, Ann. Oncol. 21 (2010) 382–388.
[7] M.E.R. O'Brien, N. Wigler, M. Inbar, R. Rosso, E. Grischke, A. Santoro, et al., Reduced cardiotoxicity and comparable efficacy in a phase III trial of pegylated liposomal doxorubicin HCl (CAELYX (TM)/Doxil (R)) versus conventional doxorubicin for first-line treatment of metastatic breast cancer, Ann. Oncol. 15 (2004) 440–449.
[8] J.V. Jokerst, T. Lobovkina, R.N. Zare, S.S. Gambhir, Nanoparticle PEGylation for imaging and therapy, Nanomedicine Lond. U. K. 6 (2011) 715–728.
[9] X.P. Han, Z.B. Li, J. Sun, C. Luo, L. Li, Y.H. Liu, et al., Stealth CD44-targeted hyaluronic acid supramolecular nanoassemblies for doxorubicin delivery: probing the effect of uncovalent pegylation degree on cellular uptake and blood long circulation, J. Control. Release 197 (2015) 29–40.
[10] S. Essa, J.M. Rabanel, P. Hildgen, Characterization of rhodamine loaded PEG-g-PLA nanoparticles (NPs): effect of poly(ethylene glycol) grafting density, Int. J. Pharm. 411 (2011) 178–187.
[11] V.C. Mosqueira, P. Legrand, J.L. Morgat, M. Vert, E. Mysiakine, R. Gref, et al., Biodistribution of long-circulating PEG-grafted nanocapsules in mice: effects of PEG chain length and density, Pharm. Res. 18 (2001) 1411–1419.
[12] X.H. Xia, M.X. Yang, Y.C. Wang, Y.Q. Zheng, Q.G. Li, J.Y. Chen, et al., Quantifying the coverage density of poly(ethylene glycol) chains on the surface of gold nanostructures, ACS Nano 6 (2012) 512–522.
[13] Y. Akiyama, T. Mori, Y. Katayama, T. Niidome, The effects of PEG grafting level and injection dose on gold nanorod biodistribution in the tumor-bearing mice, J. Control. Release 139 (2009) 81–84.
[14] H.Y. Liu, T.L. Liu, H. Wang, L.L. Li, L.F. Tan, C.H. Fu, et al., Impact of PEGylation on the biological effects and light heat conversion efficiency of gold nanoshells on silica nanorattles, Biomaterials 34 (2013) 6967–6975.
[15] C. Sacchetti, K. Motamedchaboki, A. Magrini, G. Palmieri, M. Mattei, S. Bernardini, et al., Surface polyethylene glycol conformation influences the protein corona of polyethylene glycol-modified single-walled carbon nanotubes: potential implications on biological performance, ACS Nano 7 (2013) 1974–1989.
[16] J. Xie, C.J. Xu, N. Kohler, Y.L. Hou, S.H. Sun, Controlled PEGylation of monodisperse Fe_3O_4 nanoparticles for reduced non-specific uptake by macrophage cells, Adv. Mater 19 (2007) 3163–3166.
[17] J.L. Perry, K.G. Reuter, M.P. Kai, K.P. Herlihy, S.W. Jones, J.C. Luft, et al., PEGylated PRINT nanoparticles: the impact of PEG density on protein binding, macrophage association, biodistribution, and pharmacokinetics, Nano Lett. 12 (2012) 5304–5310.
[18] C.D. Walkey, J.B. Olsen, H.B. Guo, A. Emili, W.C.W. Chan, Nanoparticle size and surface chemistry determine serum protein adsorption and macrophage uptake, J. Am. Chem. Soc. 134 (2012) 2139–2147.
[19] R. Gref, M. Lück, P. Quellec, M. Marchand, E. Dellacherie, S. Harnisch, et al., 'Stealth' corona-core nanoparticles surface modified by polyethylene glycol (PEG): influences of the corona (PEG chain length and surface density) and of the core composition on phagocytic uptake and plasma protein adsorption, Colloids Surf. B 18 (2000) 301–313.
[20] H.S.S. Qhattal, T. Hye, A. Alali, X.L. Liu, Hyaluronan polymer length, grafting density, and surface poly(ethylene glycol) coating influence in vivo circulation and tumor targeting of hyaluronan-grafted liposomes, ACS Nano 8 (2014) 5423–5440.
[21] K. Shiraishi, Y. Sanada, S. Mochizuki, K. Kawano, Y. Maitani, K. Sakurai, et al., Determination of polymeric micelles' structural characteristics, and effect of the characteristics on pharmacokinetic behaviors, J. Control. Release 203 (2015) 77–84.
[22] S.D. Li, L. Huang, Pharmacokinetics and biodistribution of nanoparticles, Mol. Pharm. 5 (2008) 496–504.
[23] A. Albanese, P.S. Tang, W.C.W. Chan, The effect of nanoparticle size, shape, and surface chemistry on biological systems, Annu. Rev. Biomed. Eng. 14 (2012) 1–16.
[24] F. Alexis, E. Pridgen, L.K. Molnar, O.C. Farokhzad, Factors affecting the clearance and biodistribution of polymeric nanoparticles, Mol. Pharm. 5 (2008) 505–515.
[25] K.C.L. Black, Y.C. Wang, H.P. Luehmann, X. Cai, W.X. Xing, B. Pang, et al., Radioactive ^{198}Au-doped nanostructures with different shapes for in vivo analyses of their biodistribution, tumor uptake, and intratumoral distribution, ACS Nano 8 (2014) 4385–4394.
[26] E.A. Sykes, J. Chen, G. Zheng, W.C.W. Chan, Investigating the impact of nanoparticle size on active and passive tumor targeting efficiency, ACS Nano 8 (2014) 5696–5706.
[27] H.S. Choi, W.H. Liu, P. Misra, E. Tanaka, J.P. Zimmer, B.I. Ipe, et al., Renal clearance of quantum dots, Nat. Biotechnol. 25 (2007) 1165–1170.
[28] M. Dellian, F. Yuan, V.S. Trubetskoy, V.P. Torchilin, R.K. Jain, Vascular permeability in a human tumour xenograft: molecular charge dependence, Br. J. Cancer 82 (2000) 1513–1518.
[29] M.J. Ernsting, M. Murakami, A. Roy, S.D. Li, Factors controlling the pharmacokinetics, biodistribution and intratumoral penetration of nanoparticles, J. Control. Release 172 (2013) 782–794.
[30] C. Fang, B. Shi, Y.Y. Pei, M.H. Hong, J. Wu, H.Z. Chen, In vivo tumor targeting of tumor necrosis factor-alpha-loaded stealth nanoparticles: effect of MePEG molecular weight and particle size, Eur. J. Pharm. Sci. 27 (2006) 27–36.
[31] S.D. Perrault, C. Walkey, T. Jennings, H.C. Fischer, W.C.W. Chan, Mediating tumor targeting efficiency of nanoparticles through design, Nano Lett. 9 (2009) 1909–1915.
[32] H. Cabral, Y. Matsumoto, K. Mizuno, Q. Chen, M. Murakami, M. Kimura, et al., Accumulation of Sub-100 nm polymeric micelles in poorly permeable tumours depends on size, Nat. Nanotechnol. 6 (2011) 815–823.
[33] T.M. Sun, J.Z. Du, L.F. Yan, H.Q. Mao, J. Wang, Self-assembled biodegradable micellar nanoparticles of amphiphilic and cationic block copolymer for siRNA delivery, Biomaterials 29 (2008) 4348–4355.
[34] Y.C. Wang, S.Y. Shen, Q.P. Wu, D.P. Chen, J. Wang, G. Steinhoff, et al., Block copolymerization of ε-caprolactone and 2-methoxyethyl ethylene phosphate initiated by aluminum isopropoxide: synthesis, characterization, and kinetics, Macromolecules 39 (2006) 8992–8998.
[35] S.C. Glotzer, Some assembly required, Science 306 (2004) 419–420.
[36] H.G. Cui, Z.Y. Chen, S. Zhong, K.L. Wooley, D.J. Pochan, Block copolymer assembly via kinetic control, Science 317 (2007) 647–650.
[37] G. Gaucher, M.H. Dufresne, V.P. Sant, N. Kang, D. Maysinger, J.C. Leroux, Block copolymer micelles: preparation, characterization and application in drug delivery, J. Control. Release 109 (2005) 169–188.
[38] X.T. Shuai, H. Ai, N. Nasongkla, S. Kim, J.M. Gao, Micellar carriers based on block copolymers of poly(ε-caprolactone) and poly(ethylene glycol) for doxorubicin delivery, J. Control. Release 98 (2004) 415–426.
[39] Q. Yang, S.W. Jones, C.L. Parker, W.C. Zamboni, J.E. Bear, S.K. Lai, Evading immune cell uptake and clearance requires PEG grafting at densities substantially exceeding the minimum for brush conformation, Mol. Pharm. 11 (2014) 1250–1258.
[40] V.B. Damodaran, C.J. Fee, T. Ruckh, K.C. Popat, Conformational studies of covalently grafted poly(ethylene glycol) on modified solid matrices using X-ray photoelectron spectroscopy, Langmuir 26 (2010) 7299–7306.
[41] E.A. Nance, G.F. Woodworth, K.A. Sailor, T.Y. Shih, Q.G. Xu, G. Swaminathan, et al., A dense poly(ethylene glycol) coating improves penetration of large polymeric nanoparticles within brain tissue, Sci. Transl. Med. 4 (2012) 149ra119.
[42] Y. Liu, Y.X. Hu, L. Huang, Influence of polyethylene glycol density and surface lipid on pharmacokinetics and biodistribution of lipid-calcium-phosphate nanoparticles, Biomaterials 35 (2014) 3027–3034.
[43] J.W. Baish, T. Stylianopoulos, R.M. Lanning, W.S. Kamoun, D. Fukumura, L.L. Munn, et al., Scaling rules for diffusive drug delivery in tumor and normal tissues, Proc. Natl. Acad. Sci. U. S. A. 108 (2011) 1799–1803.
[44] Y. Matsumura, H. Maeda, A new concept for macromolecular therapeutics in cancer-chemotherapy - mechanism of tumoritropic accumulation of proteins and the antitumor agent smancs, Cancer Res. 46 (1986) 6387–6392.
[45] R. Misra, S. Acharya, S.K. Sahoo, Cancer nanotechnology: application of nanotechnology in cancer therapy, Drug Discov. Today 15 (2010) 842–850.
[46] Y. Li, R.Y. Liu, J. Yang, Y.J. Shi, G.H. Ma, Z.Z. Zhang, et al., Enhanced retention and anti-tumor efficacy of liposomes by changing their cellular uptake and pharmacokinetics behavior, Biomaterials 41 (2015) 1–14.
[47] S. Mishra, P. Webster, M.E. Davis, PEGylation significantly affects cellular uptake and intracellular trafficking of non-viral gene delivery particles, Eur. J. Cell Biol. 83 (2004) 97–111.
[48] X.Z. Yang, X.J. Du, Y. Liu, Y.H. Zhu, Y.Z. Liu, Y.P. Li, et al., Rational design of polyion complex nanoparticles to overcome cisplatin resistance in cancer therapy, Adv. Mater 26 (2014) 931–936.
[49] J. Zhao, S.S. Feng, Effects of PEG tethering chain length of vitamin E TPGS with a Herceptin-functionalized nanoparticle formulation for targeted delivery of anticancer drugs, Biomaterials 35 (2014) 3340–3347.
[50] Y. Hu, J.W. Xie, Y.W. Tong, C.H. Wang, Effect of PEG conformation and particle size on the cellular uptake efficiency of nanoparticles with the HepG2 cells, J. Control. Release 118 (2007) 7–17.
[51] M. Miteva, K.C. Kirkbride, K.V. Kilchrist, T.A. Werfel, H.M. Li, C.E. Nelson, et al., Tuning PEGylation of mixed micelles to overcome intracellular and systemic siRNA delivery barriers, Biomaterials 38 (2015) 97–107.
[52] S. Hak, E. Helgesen, H.H. Hektoen, E.M. Huuse, P.A. Jarzyna, W.J.M. Mulder, et al., The effect of nanoparticle polyethylene glycol surface density on ligand-directed tumor targeting studied in vivo by dual modality imaging, ACS Nano 6 (2012) 5648–5658.